

15. M. Tucci et al., *J. Endocrinol.* **157**, 13 (1998).  
 16. T. Oono et al., *J. Invest. Dermatol.* **100**, 329 (1993).  
 17. E. Jendraschak and E. H. Sage, *Semin. Cancer Biol.* **7**, 139 (1996).  
 18. N. Bardin et al., *Tissue Antigens* **48**, 531 (1996).  
 19. D. M. Bradham, A. Igarashi, R. L. Potter, G. R. Groten-dorst, *J. Cell Biol.* **114**, 1285 (1991).  
 20. K. Akaogi et al., *Proc. Natl. Acad. Sci. U.S.A.* **93**, 8384 (1996).  
 21. Y. Muragaki et al., *Proc. Natl. Acad. Sci. U.S.A.* **92**, 8763 (1995).  
 22. M. L. Iruela-Arispe, C. A. Diglio, E. H. Sage, *Arterio-scler. Thromb.* **11**, 805 (1991).  
 23. J. P. Girard and T. A. Springer, *Immunity* **2**, 113 (1995).  
 24. E. A. Jaffe et al., *J. Immunol.* **143**, 3961 (1989).  
 25. J. P. Girard et al., *Am. J. Pathol.* **155**, 2043 (1999).  
 26. H. Ohtani and N. Sasano, *J. Electron Microsc.* **36**, 204 (1987).  
 27. For nonradioactive in situ hybridization, digoxigenin (DIG)-labeled antisense RNA probes were generated by PCR amplification of 500- to 600-bp products and incorporation of a T7 promoter into the antisense primer. In vitro transcription was performed with DIG RNA labeling reagents and T7 RNA polymerase (Roche, Indianapolis, IN). Frozen tissue sections were fixed with 4% paraformaldehyde, permeabilized with pepsin, and incubated with RNA probe (200 ng/ml) overnight at 55°C. For signal amplification, a horse-radish peroxidase (HRP) rabbit anti-DIG antibody (DAKO, Carpinteria, CA) was used to catalyze the deposition of Biotin-Tyramide (GenPoint kit, DAKO). Further amplification was achieved by adding HRP rabbit anti-biotin (DAKO), biotin-tyramide, and then alkaline-phosphatase (AP) rabbit anti-biotin (DAKO). Signal was detected with the AP substrate Fast Red TR/Naphthol AS-MX (Sigma, St. Louis, MO), and cells were counterstained with hematoxylin unless otherwise indicated. A detailed protocol including the list of primers used to generate the probes can be obtained from the authors upon request.  
 28. Differentially expressed endothelial-specific transcripts were defined as those expressed at levels at least fivefold higher in ECs in vivo than in nonendothelial cell lines in culture (14) and present at no more than five copies per 100,000 transcripts in nonendothelial cell lines and the hematopoietic cell fraction (39). Transcripts showing statistically different levels of expression ( $P < 0.05$ ) were then identified by Monte Carlo analysis (40). Transcripts preferentially expressed in normal endothelium were then defined as those expressed at levels at least 10-fold higher in normal endothelium than in tumor endothelium. Conversely, tumor endothelial transcripts were present at levels at least 10-fold higher in tumor versus normal endothelium. See [www.sagenet.org/angio/table2.htm](http://www.sagenet.org/angio/table2.htm) and [www.sagenet.org/angio/table3.htm](http://www.sagenet.org/angio/table3.htm) for a complete list of differentially expressed genes.  
 29. M. Iurlaro et al., *Eur. J. Clin. Invest.* **29**, 793 (1999).  
 30. W. S. Lee et al., *Circ. Res.* **82**, 845 (1998).  
 31. J. Niquet and A. Represa, *Brain. Res. Dev. Brain Res.* **95**, 227 (1996).  
 32. L. Fouser, L. Iruela-Arispe, P. Bornstein, E. H. Sage, *J. Biol. Chem.* **266**, 18345 (1991).  
 33. M. L. Iruela-Arispe, P. Hasselaar, H. Sage, *Lab Invest.* **64**, 174 (1991).  
 34. See [www.sagenet.org/angio/table4.htm](http://www.sagenet.org/angio/table4.htm).  
 35. H. F. Dvorak, *N. Engl. J. Med.* **315**, 1650 (1986).  
 36. N. A. Datson, J. van der Perk-de Jong, M. P. van den Berg, E. R. de Kloet, E. Vreugdenhil, *Nucleic Acids Res.* **27**, 1300 (1999).  
 37. B. Virlon et al., *Proc. Natl. Acad. Sci. U.S.A.* **96**, 15286 (1999).  
 38. V. E. Velculescu et al., *Nature Genet.* **23**, 387 (1999).  
 39. Human colon tissues were obtained <30 min after surgical removal. Normal tissue was taken from regions >10 cm away from bulk tumor tissue that had clearly defined margins. For normal tissue, sheets of epithelial cells were removed with a glass slide after treatment with 5 mM dithiothreitol, then 10 mM EDTA, leaving an intact lamina propria for subsequent processing. After a 2-hour incubation in collagenase at 37°C, cells were filtered sequentially through 400-, 100-, 50-, and 25- $\mu$ m mesh and centrifuged through a 30% preformed Percoll gradient to sediment red

blood cells. Epithelial cells (Epithelial Fraction), which were found to nonspecifically bind magnetic beads, were removed with Dynabeads coupled to BerEP4 (DynaL, Lake Success, NY). Subsequently, macrophages and other leukocytes (Hematopoietic Fraction) were removed with a mixture of beads coupled to anti-CD45, anti-CD14, and anti-CD64 (DynaL). The remaining cells were stained with P1H12 antibody, purified with anti-mouse immunoglobulin G (IgG)-coupled magnetic beads, and lysed in mRNA lysis buffer. A detailed protocol can be obtained from [www.sagenet.org/angio/protocol.htm](http://www.sagenet.org/angio/protocol.htm).  
 40. L. Zhang et al., *Science* **276**, 1268 (1997).  
 41. H. Sheikh, H. Yarwood, A. Ashworth, C. M. Isacke, *J. Cell Sci.* **113**, 1021 (2000).  
 42. We thank L. Meszler (Johns Hopkins Oncology Cell Imaging Facility) for expert help with the microscopic imaging and S. Kern and R. Hruban for pancreatic cancer samples. Supported by NIH grants CA57345, CA62924,

and CGAP S98-146A. B.S.C. is a research Fellow of the National Cancer Institute of Canada supported with funds provided from the Terry Fox Run. K.W.K. received research funding from Genzyme Molecular Oncology (Genzyme). Under a licensing agreement between the Johns Hopkins University and Genzyme, the SAGE technology was licensed to Genzyme for commercial purposes, and V.V., B.V., and K.W.K. are entitled to a share of royalty received by the university from sales of the licensed technology. The SAGE technology is freely available to academia for research purposes. V.V., B.V., and K.W.K. are consultants to Genzyme. The university and researchers (V.V., B.V., and K.W.K.) own Genzyme stock, which is subject to certain restrictions under university policy. The terms of these arrangements are being managed by the university in accordance with its conflict of interest policies.

15 May 2000; accepted 28 June 2000

## Inflammation Dampened by Gelatinase A Cleavage of Monocyte Chemoattractant Protein-3

G. Angus McQuibban,<sup>1</sup> Jiang-Hong Gong,<sup>2</sup> Eric M. Tam,<sup>1</sup> Christopher A. G. McCulloch,<sup>4</sup> Ian Clark-Lewis,<sup>2</sup> Christopher M. Overall<sup>1,3\*</sup>

Tissue degradation by the matrix metalloproteinase gelatinase A is pivotal to inflammation and metastases. Recognizing the catalytic importance of substrate-binding exosites outside the catalytic domain, we screened for extracellular substrates using the gelatinase A hemopexin domain as bait in the yeast two-hybrid system. Monocyte chemoattractant protein-3 (MCP-3) was identified as a physiological substrate of gelatinase A. Cleaved MCP-3 binds to CC-chemokine receptors-1, -2, and -3, but no longer induces calcium fluxes or promotes chemotaxis, and instead acts as a general chemokine antagonist that dampens inflammation. This suggests that matrix metalloproteinases are both effectors and regulators of the inflammatory response.

Degradomics, the identification of biologically relevant substrates for the increasing number of recognized proteinases, is a challenge of proteomics. Although yeast two-hybrid screening (1) has identified intracellular protein-protein interactions, a screening rationale with a proteinase catalytic domain as target is tenuous because cleavage of library-encoded substrate would preclude detection. Therefore, to identify potential matrix metalloproteinase (MMP) substrates, we used a substrate-binding exosite domain, the hemopexin COOH-terminal (C) domain (2, 3), that is structurally and functionally distinct from the catalytic domain in a two-hybrid screen. Collagen binding by this domain

of collagenolytic MMPs is a prerequisite for cleavage. Therefore, other proteins that bind to this domain may also be MMP substrates.

To determine the suitability of the two-hybrid system for extracellular proteins, we assessed the interaction between the single-disulfide-bonded gelatinase A (MMP-2) hemopexin C domain and the C domain of the tissue inhibitor of metalloproteinase-2 (TIMP-2), which contains three disulfide bonds. Deletion (4) and domain-swapping (5) studies indicate that these domains interact in the cellular activation and localization of gelatinase A to cell surface membrane type (MT)-MMPs (6). Association was detected (Fig. 1, A and B), indicating that in yeast at 30°C, a stable, functional protein fold in domains that normally contain disulfide bonds was achieved.

A cDNA library was constructed from human gingival fibroblasts treated with concanavalin A (Con A), a stimulant of extracellular matrix degradation through the activation of gelatinase A (7). Using the human

<sup>1</sup>Department of Biochemistry and Molecular Biology, <sup>2</sup>Biomedical Research Centre, <sup>3</sup>Department of Oral Biological and Medical Sciences, University of British Columbia, Vancouver, BC V6T 1Z3, Canada. <sup>4</sup>Medical Research Council Group in Periodontal Physiology, University of Toronto, Toronto, ON M5S 3E8, Canada.

\*To whom correspondence should be addressed. E-mail: overall@interchange.ubc.ca

REPORTS

gelatinase A hemopexin C domain in yeast two-hybrid screens, we identified monocyte chemoattractant protein-3 (MCP-3) as a potential binding protein (Fig. 1, A and B). MCP-3 is one of several tissue-derived CC-chemokines that recruits monocytes and other leukocytes in inflammation and osteosarcoma (8). The hemopexin C domain had a comparable interaction with both MCP-3 and the TIMP-2 C domain (Fig. 1B). Chemical cross-linking of synthetic MCP-3 to recombinant hemopexin C domain verified this interaction (Fig. 1C). The cross-linked MCP-3-hemopexin C domain had the mass of a 1:1 bimolecular complex, whereas MCP-3 alone was not cross-linked. Furthermore, the hemopexin C domain showed saturable binding to MCP-3 by an enzyme-linked immunosorbent assay (ELISA)-based binding assay (Fig. 1D). Absence of binding by recombinant gelatinase A collagen binding domain (9) composed of three fibronectin type II modules confirmed specificity. Full-length gelatinase A also bound MCP-3 (Fig. 2A), whereas truncated gelatinase A lacking the hemopexin C domain (N-gelatinase A) did not (Fig. 2B). No interaction was observed between gelatinase A and the related CC-chemokine, MCP-1. As controls, full-length and N-gelatinase A did bind to gelatin and TIMP-2 by the collagen binding domain and active site (10), respectively. Hence, these data demonstrate a specific requirement for the hemopexin C domain of gelatinase A for binding MCP-3.

Incubation of MCP-3 with recombinant gelatinase A resulted in a small but distinct increase in electrophoretic mobility of MCP-3 on tricine gels (Fig. 2C) that was blocked by the MMP-specific inhibitor TIMP-2 and the hydroxamate inhibitor BB-2275. Exogenous recombinant gelatinase A hemopexin C domain decreased MCP-3 cleavage, whereas the collagen binding domain had no effect (Fig. 2C). In addition, the  $k_{cat}/K_m$  decreased from 8000  $M^{-1} s^{-1}$  for full-length gelatinase A cleavage of MCP-3 to 500  $M^{-1} s^{-1}$  for N-gelatinase A, confirming the mechanistic importance of the hemopexin C domain exosite in MCP-3 degradation. These kinetic parameters for full-length gelatinase A cleavage of MCP-3 were higher than for denatured type I collagen (gelatin), 7580  $M^{-1} s^{-1}$  (11), indicating that MCP-3 should be efficiently cleaved in vivo. Indeed, MCP-3 but not MCP-1 was cleaved by cultured human fibroblasts after Con A-induced gelatinase A activation (Fig. 2D). Cleavage of MCP-3 by other MMPs was also examined (12). Although gelatinase A was the most efficient of these proteinases, collagenase-3 (MMP-13) and MT1-MMP (MMP-14) also processed MCP-3, further favoring the cleavage of MCP-3 in vivo. However, MCP-3 was not a general MMP substrate

**Fig. 1.** MCP-3 interactions with the gelatinase A hemopexin C domain (Hex CD). (A) In the yeast two-hybrid assay only the yeast transformants Hex CD/TIMP-2 CD, Hex CD/MCP-3, and p53/SV40 (positive control) showed growth on medium lacking histidine. (B)  $\beta$ -Galactosidase levels in yeast expressing the indicated fusion proteins. (C) Cross-linking of MCP-3 and recombinant hemopexin C domain. MCP-3 alone, or in the presence of 0.5 M equivalent (+), 1.0 M equivalent (++), or 2.0 M equivalents (+++) of hemopexin C domain, was cross-linked with 0.5% glutaraldehyde for 20 min at 22°C. (D) ELISA binding assay of 0.5  $\mu$ g of MCP-3 immobilized onto a 96-well plate and then incubated with recombinant gelatinase A hemopexin C domain or collagen binding domain (CBD).

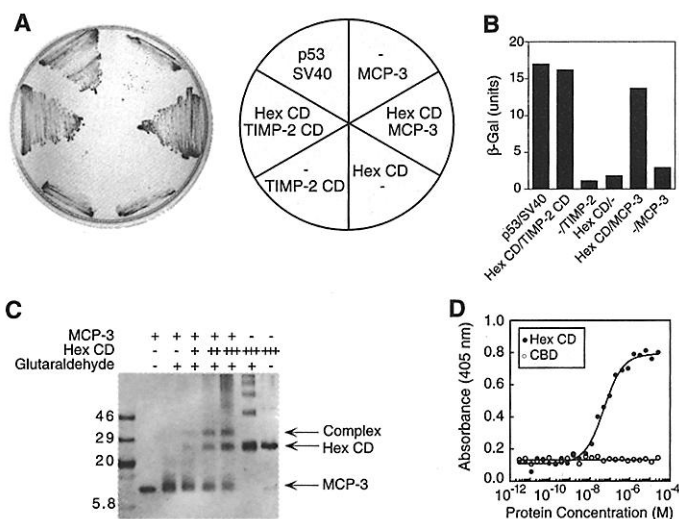
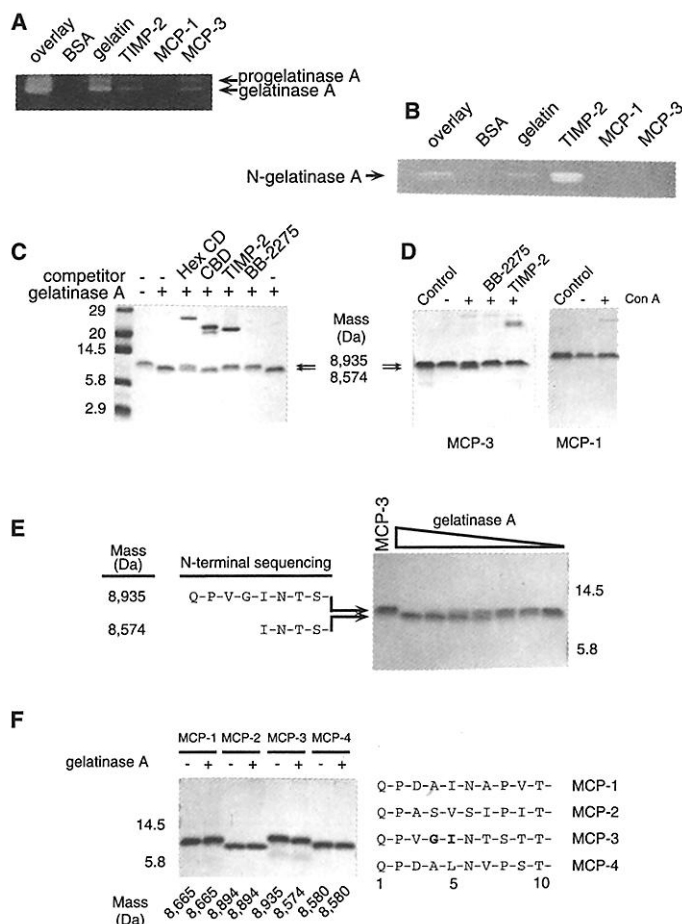


**Fig. 2.** Gelatinase A binding and cleavage of MCP-3. (A) Gelatin zymography of enzyme capture film assay of pro- and active gelatinase A. Five micrograms each of bovine serum albumin (BSA), gelatin, TIMP-2, MCP-1, and MCP-3 were immobilized onto a 96-well plate. Recombinant gelatinase A was then overlaid for 2 hours and the bound protein analyzed by zymography. Overlay, recombinant enzyme used. (B) Gelatin zymography as in (A), but with hemopexin C domain-truncated gelatinase A (N-gelatinase A) used as overlay. (C) Tricine gel analysis of MCP-3 cleavage by gelatinase A in the presence of equimolar amounts (relative to MCP-3) of recombinant hemopexin C domain (Hex CD), collagen binding domain (CBD), TIMP-2, or 10  $\mu$ M BB-2275 (British Biotech Pharmaceuticals, Oxford, United Kingdom). (D) Tricine gel analysis of human fibroblast-mediated MCP-3 cleavage. Fibroblast cultures were treated with Con A for 24 hours at 37°C. After a 16-hour incubation with MCPs in the presence of the MMP inhibitors indicated [concentrations as in (C)], the conditioned culture media were analyzed by tricine SDS-polyacrylamide gel electrophoresis (PAGE). The masses of the MCP-3 forms in the culture media were measured by electrospray mass spectrometry. (E) Electrospray mass spectrometry,  $NH_2$ -terminal Edman sequencing, and tricine gel analysis of MCP-3 cleavage products produced by recombinant gelatinase A activity. MCP-3 (5  $\mu$ g) was incubated with 100 ng, 10 ng, 1 ng, 100 pg, 10 pg, 1 pg, or 100 fg of recombinant gelatinase A for 4 hours at 37°C. (F) Electrospray mass spectrometry and tricine gel analysis of MCP-1, -2, -3, and -4 after incubation with recombinant gelatinase A for 18 hours at 37°C. The  $NH_2$ -terminal sequence of the MCPs is shown with the Gly-Ile scissile bond in MCP-3 in bold.



because matrilysin (MMP-7), which lacks a hemopexin C domain, and the leukocyte MMPs—collagenase-2 (MMP-8) and gelatinase B (MMP-9)—did not cleave MCP-3.

To identify the cleavage site in MCP-3,

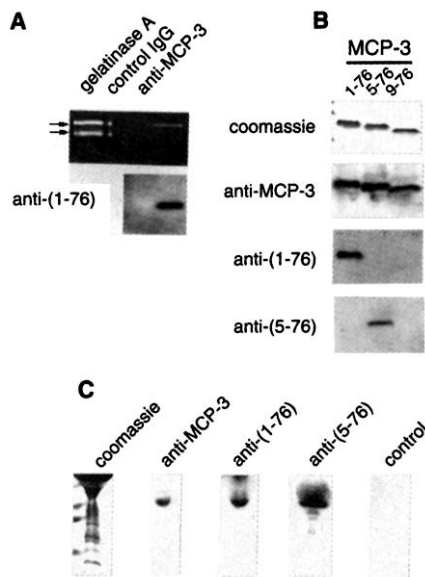


**Fig. 3.** Identification of in vivo human MCP-3-progelatinase A complexes and cleaved MCP-3(5-76) in human synovial fluid. (A) MCP-3 was immunoprecipitated with an anti-MCP-3 monoclonal antibody from 200  $\mu$ l of synovial fluid of a patient with seronegative spondyloarthritis. Gelatin zymography (top) and Western blotting with rabbit anti-MCP-3(1-76) (bottom) of the complexes. (B) Characterization of affinity-purified antibody raised against residues one to five of MCP-3 [anti-(1-76)] and the neoepitope at residues five to nine of MCP-3 [anti-(5-76)]. (C) Identification of MCP-3(5-76) in human rheumatoid synovial fluid. Total protein is shown after SDS-PAGE and Coomassie staining. Detection of full-length and gelatinase A-cleaved forms of MCP-3 in human synovial fluid by Western blotting with antibodies as indicated. Control blot indicates anti-(5-76) preadsorbed with synthetic MCP-3(5-76) before use.

we performed electrospray mass spectrometry. The mass of the gelatinase A-cleaved MCP-3 was 8574 daltons both in vivo (Fig. 2D) and in vitro (Fig. 2, C and E), a reduction from the mass of the full-length molecule (8935 daltons) by the exact mass of the NH<sub>2</sub>-terminal four residues. NH<sub>2</sub>-terminal Edman sequencing confirmed the scissile bond to be Gly<sup>4</sup>-Ile<sup>5</sup> (Fig. 2E), a preferred sequence for gelatinase A cleavage (13) that is absent in other MCPs not cleaved by gelatinase A (Fig. 2F), including mouse MCP-3 (12).

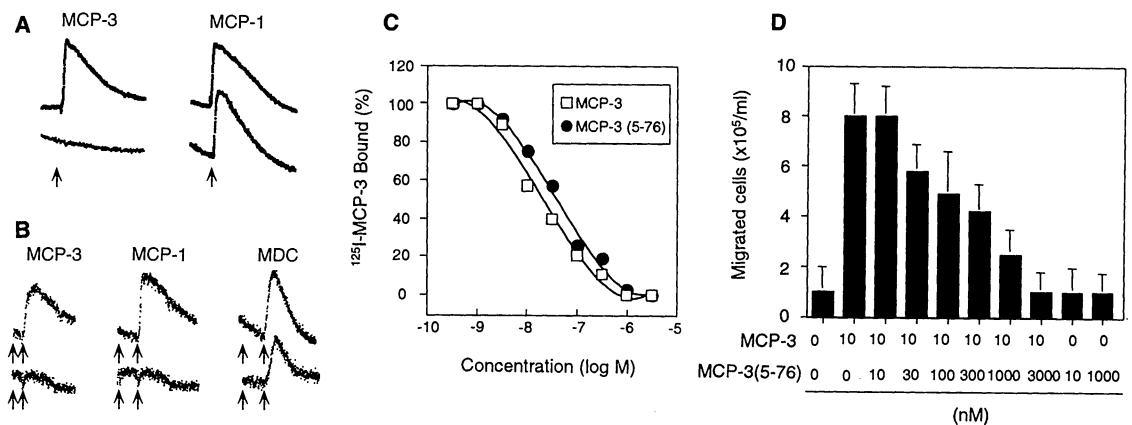
A monoclonal antibody to human MCP-3 coimmunoprecipitated progelatinase A, but not the active enzyme, from the synovial fluid of an arthritis patient (Fig. 3A). Full-length MCP-3 was identified in these immunocomplexes with an affinity-purified antibody raised against the NH<sub>2</sub>-terminal five residues of MCP-3 (Fig. 3A). Gelatinase A-cleaved MCP-3 was also detected in human rheumatoid synovial fluids with affinity-purified anti-neoepitope antibody that recognizes the free amino group of the cleaved MCP-3 at Ile<sup>5</sup>, but not the full-length MCP-3 nor another truncated MCP-3 (residues 9 to 76) used as controls (Fig. 3, B and C). Hence, these data demonstrate that MCP-3 interacts with and is cleaved by gelatinase A in vivo.

MCP-3 binds leukocyte CC-receptor-1 (CCR-1), -2, and -3 and mobilizes intracellular calcium, resulting in directed cell migration of leukocytes. NH<sub>2</sub>-terminal truncation of synthetic MCP-1 and MCP-3 at different sites has variable effects on their agonist activity (14, 15). Gelatinase A-mediated removal of the first four residues of MCP-3 resulted in the loss of CCR-1 and -2 activation in THP-1 cells (16), a monocyte cell line that expresses these two receptors. Neither gelatinase A-cleaved MCP-3 in the presence of 1/1000 (mole ratio) gelatinase A (Fig. 4A) nor synthetic MCP-3(5-76) (MCP-3 residues 5 to 76, corresponding to the gelatinase A-cleaved form) (Fig. 4B) elicited a calcium response. In

addition to loss of CCR agonist activity, MCP-3(5-76) antagonized the subsequent response not only to MCP-3, but also to MCP-1 (Fig. 4B) and macrophage inflammatory protein-1 $\alpha$  (MIP-1 $\alpha$ ) (17). MCP-1 only binds CCR-2 and MIP-1 $\alpha$  binds to CCR-1 and CCR-5, confirming the CCR-1 and CCR-2 antagonist activity of MCP-3(5-76). MCP-3(5-76) did not block the calcium response to macrophage-derived chemokine (MDC), which binds CCR-4, a receptor not bound by MCP-3 (Fig. 4B). The physiological relevance of MCP-3 antagonism was confirmed by cell-binding assays (18). Scatchard analysis showed that synthetic MCP-3(5-76) bound THP-1 cells with high affinity [dissociation constant ( $K_d$ ) = 18.3 nM], similar to that of full-length MCP-3 ( $K_d$  = 5.7 nM) (Fig. 4C). In transwell cell migration assays (19), MCP-3(5-76) was not chemotactic, even in amounts 100-fold higher than full-length MCP-3 (Fig. 4D). MCP-3(5-76) also functioned as an antagonist in a dose-dependent manner to inhibit the chemotaxis directed by full-length chemokine (Fig. 4D). Thus, MMP inactivation of MCP-3 also generates a broad-spectrum antagonist for CC-receptors that retains strong cellular binding affinity and modulates the response to a number of related chemoattractants.

To examine the biological effects of gelatinase A cleavage of MCP-3 in inflammation, we injected various mole ratios of full-length MCP-3 and gelatinase A-cleaved or synthetic MCP-3(5-76) into mice subcutaneously (20). Full-length, but not cleaved MCP-3, induced infiltration of mononuclear inflammatory cells with associated matrix degradation at 18 hours after injection (Fig. 5, A to D). A statistically significant reduction in the mononuclear cell infiltrate in response to as little as a 1:1 mixture of MCP-3(5-76) with MCP-3 was observed (Fig. 5E). In a separate mouse model of inflammation, the cellular infiltrate in 24-hour zymosan A-induced peritonitis (21) was attenuated after intraperitoneal injection with MCP-3(5-

**Fig. 4.** Cellular responses to gelatinase A-cleaved MCP-3. (A) Loss of intracellular calcium mobilization by MCP-3 after gelatinase A cleavage. Fluo-3AM-loaded THP-1 monocytes were treated (arrows) with 5 nM MCP-3 or MCP-1 (top scans) or the respective chemokine incubated first with gelatinase A for 18 hours (bottom scans). The data are presented as relative fluorescence emitted at 526 nm. (B) Intracellular calcium mobilization by MCP-3, MCP-1, and MDC. Fluo-3AM-loaded THP-1 monocytes or a B-cell line transfected with CCR-4 (for MDC) were first exposed to either 0 nM (left arrow, top scans) or 500 nM MCP-3(5-76) (left arrow, bottom scans), followed by MCP-3 (30 nM),



MCP-1 (5 nM), or MDC (5 nM), as indicated (right arrow, top and bottom scans). (C) THP-1 cell receptor binding of MCP-3 and MCP-3(5-76). (D) Transwell assay of monocytes treated with MCP-3 and MCP-3(5-76) at the indicated amounts.

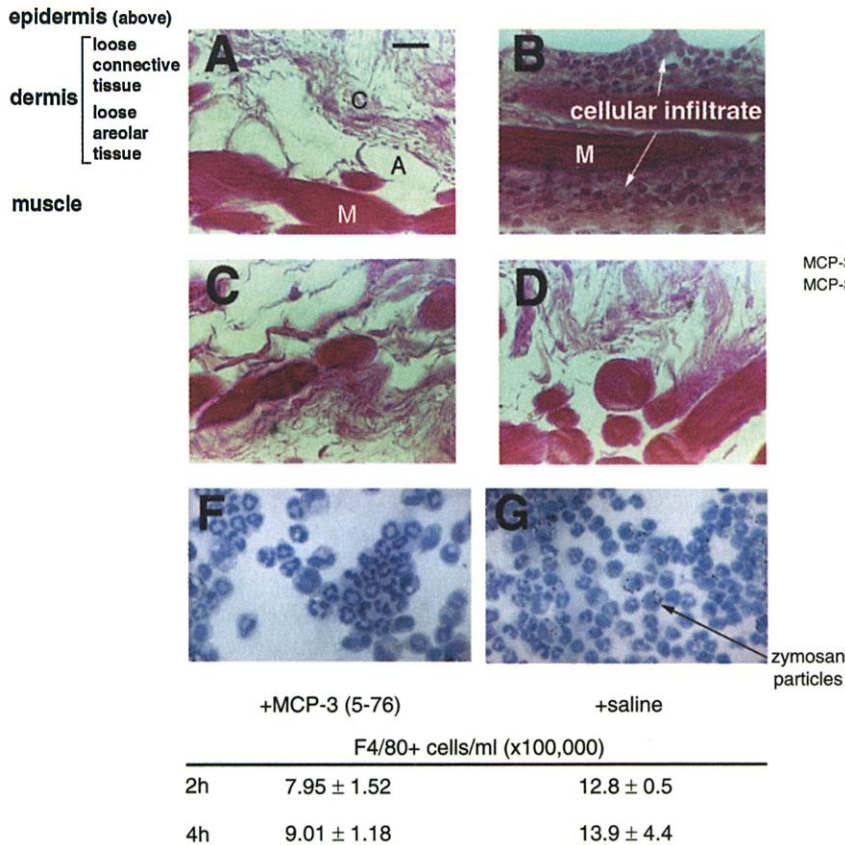


**Fig. 5.** Animal responses to gelatinase A-cleaved MCP-3. Light micrographs of H&E-stained subcutaneous tissue sections (tissue region as shown) of mice injected with (A) saline/buffer control M, muscle; A, adipocyte; C, loose connective tissue. Bar, 20  $\mu\text{m}$ ., (B) MCP-3, (C) gelatinase A-cleaved MCP-3, or (D) 2:1 molar ratio of gelatinase A-cleaved MCP-3:full-length MCP-3. (E) After subcutaneous injections with MCP-3 and MCP-3(5-76) mixtures, the infiltrating mononuclear cells were enumerated and expressed as cells per 75,000  $\mu\text{m}^2$  ( $n = 5$ , mean  $\pm$  SD;  $P < 0.01$  compared with MCP-3). (F and G) H&E-stained cytopsin washouts of intraperitoneal washouts of zymosan A-treated mice injected 24 hours later with (F) MCP-3(5-76) or (G) saline for 4 hours. Macrophage cell counts by flow cytometric analysis for each group of mice are presented below ( $n = 5$ , mean  $\pm$  SD;  $P < 0.05$  by analysis of variance).

76). Consistent with morphometric examination of the cell content in the peritoneal cavity (Fig. 5, F and G), flow cytometric analysis (22) of peritoneal washouts showed that macrophage (F4/80+) cell counts were reduced by ~40% at both 2 and 4 hours after MCP-3(5-76) treatment (Fig. 5, F and G).

Chemokine inactivation and clearance in vivo is not well understood (23). Although several examples are known in which metalloproteinase activity activates cytokines (24) and  $\alpha$ -defensins (25), this study demonstrates the extracellular inactivation of a cytokine in vivo by MMP activity. The relative amounts of intact and cleaved MCP-3 that are present after pathophysiological cleavage regulate chemotaxis and the extent of inflammation. Identification of the importance of gelatinase A in the pathophysiological processing of MCP-3 reveals the intersection of two distinct pathways that regulate the extracellular environment and the immune response. MMP expression is induced at foci of inflammation by leukocytic and stromal-derived cytokines. Notably, gelatinase A is derived largely from stromal cells and is not usually expressed by leukocytes (26); these cells express MMP-8 and gelatinase B, both of which do not cleave MCP-3. Therefore, leukocyte proteolytic activity is unlikely to disrupt cognate chemokine gradients. Overall, the activity of several tissue-derived MMPs, and gelatinase A in particular, can contribute to the cessation of

the host response, an important aspect of healing and tissue resolution. Because TGF- $\beta$ 1, a growth factor that orchestrates wound repair (27), stimulates gelatinase A but represses other MMPs (28), the interactions of MMPs with chemokines provide a self-attenuating network to dissipate proinflammatory activities. Therefore, MMPs are both effectors and regulators of inflammation.

**References and Notes**

1. S. Fields and O. Song, *Nature* **340**, 245 (1988).
2. F. X. Gomis-Ruth et al., *J. Mol. Biol.* **264**, 556 (1996).
3. U. M. Wallon and C. M. Overall, *J. Biol. Chem.* **272**, 747 (1997).
4. R. V. Ward, S. J. Atkinson, J. J. Reynolds, G. Murphy, *Biochem. J.* **304**, 263 (1994).
5. Q. Nguyen et al., *Biochemistry* **33**, 2089 (1994).
6. H. Sato et al., *Nature* **370**, 61 (1994).
7. C. M. Overall and J. Sodek, *J. Biol. Chem.* **265**, 21141 (1990).
8. G. Opendakker et al., *Biochem. Biophys. Res. Commun.* **191**, 535 (1993).
9. B. Steffensen, U. M. Wallon, C. M. Overall, *J. Biol. Chem.* **270**, 11555 (1995).
10. E. W. Howard, E. C. Bullen, M. J. Banda, *J. Biol. Chem.* **266**, 13064 (1991).
11. T. N. Young, S. V. Pizzo, S. Stack, *J. Biol. Chem.* **270**, 999 (1995).
12. G. A. McQuibban and C. M. Overall, unpublished data.
13. S. Netzel-Arnett et al., *Biochemistry* **32**, 6427 (1993).
14. J.-H. Gong and I. Clark-Lewis, *J. Exp. Med.* **181**, 631 (1995).
15. J.-H. Gong et al., *J. Biol. Chem.* **271**, 10521 (1996).
16. The fluorescence of Fluo-3AM-loaded cells was monitored with a Perkin-Elmer 650-10B spectrofluorimeter (excitation wavelength 506 nm, emission wavelength 526 nm). Desensitization assays were performed by sequential addition of

MCP-3(5-76) or buffer control, followed by the full-length chemokine.

17. G. A. McQuibban, J.-H. Gong, I. Clark-Lewis, C. M. Overall, unpublished data.
18.  $^{125}\text{I}$ -Labeled MCP-3 (4 nM) in the presence of serially diluted unlabeled MCP-3 or MCP-3(5-76) and 0.05%  $\text{Na}_2\text{S}_2\text{O}_8$  was incubated at 4°C for 30 min with THP-1 cells. Cell-bound and free  $^{125}\text{I}$ -MCP-3 were separated by centrifugation of the cells through a column of dioctyl phthalate:*n*-butyl phthalate (2:3, v/v). Bound  $^{125}\text{I}$ -labeled MCP-3 in the cell pellet was measured by gamma counting. Nonspecific binding was determined in the presence of a 100-fold concentration of unlabeled ligand and was subtracted from the total.
19. THP-1 cell migration was assessed in transwell trays (Costar; 6.5-mm diameter, 3- $\mu\text{m}$  membrane pore size). Chemokines were added to the lower well and THP-1 cells ( $1 \times 10^7$  cells per milliliter) were added to the upper well. After 1.5 hours, cells that had migrated to the lower well were counted.
20. CD-4 mice (five per group) were injected at two subcutaneous sites (500 ng/100  $\mu\text{l}$  of pyrogen-free saline) with chemokine, as indicated. In other experiments, five mice per group were injected as before, but with mixtures of 100  $\mu\text{l}$  of MCP-3 and synthetic MCP-3(5-76). Mice were killed 18 hours after injection, and paraffin sections transverse to the skin were analyzed after hematoxylin and eosin (H&E) staining for mononuclear cells.
21. Peritonitis, with an associated 40-fold increase in inflammatory cell numbers, was induced in mice by using zymosan A. Fifty micrograms of MCP-3(5-76) or saline was administered to the peritoneal cavity after 24 hours. Infiltrating cells were collected after 2 and 4 hours by saline lavage. Cells were counted on a Coulter Counter gated at 5 to 10  $\mu\text{m}$ . Cytopsin (100  $\mu\text{l}$ ) were examined by light microscopy after H&E staining.
22. Peritoneal inflammatory cells were stained for 60 min on ice with rat anti-mouse F4/80 monoclonal antibody or rat IgG2b isotype control (each at 20

μg/ml). After washing, cells were stained with fluorescein isothiocyanate-conjugated anti-rat immunoglobulin G for 45 min on ice, washed, and analyzed by flow cytometry with a FACScan analyzer (Becton Dickinson, Oxford, UK).

23. J. Van Damme et al., *Chem. Immunol.* **72**, 42 (1999).

24. A. J. Gearing et al., *Nature* **370**, 555 (1994).

25. C. L. Wilson et al., *Science* **286**, 113 (1999).

26. G. Openakker, S. Masure, B. Grillet, J. Van Damme, *Lymphokine Cytokine Res.* **10**, 317 (1991).

27. J. J. Letterio and A. B. Roberts, *Annu. Rev. Immunol.* **16**, 137 (1998).

28. C. M. Overall, J. L. Wraha, J. Sodek, *J. Biol. Chem.* **266**, 14064 (1991).

29. We thank G. Pelman for synovial fluid samples. Supported by a grant from the National Cancer Institute of Canada (NCIC), with funds provided in part by the Canadian Cancer Society, and by Medical Research Council Group grant funding. G.A.M. is supported by a NCIC studentship.

2 May 2000; accepted 30 June 2000

# Modulation of Human Visual Cortex by Crossmodal Spatial Attention

Emiliano Macaluso,<sup>1,2\*</sup> Chris D. Frith,<sup>2</sup> Jon Driver<sup>1</sup>

A sudden touch on one hand can improve vision near that hand, revealing crossmodal links in spatial attention. It is often assumed that such links involve only multimodal neural structures, but unimodal brain areas may also be affected. We tested the effect of simultaneous visuo-tactile stimulation on the activity of the human visual cortex. Tactile stimulation enhanced activity in the visual cortex, but only when it was on the same side as a visual target. Analysis of effective connectivity between brain areas suggests that touch influences unimodal visual cortex via back-projections from multimodal parietal areas. This provides a neural explanation for crossmodal links in spatial attention.

Spatial attention picks out particular locations for further sensory processing. Most studies of spatial attention have considered only a single sensory modality at a time (1, 2), but crossmodal links have now been demonstrated psychophysically. For instance, a tactile cue at one location can improve discrimination for visual stimuli at that location relative to others (3, 4). This crossmodal effect arises even if the tactile cues are task-irrelevant and do not predict the location of the visual targets, suggesting an exogenous (stimulus-driven) attentional mechanism. The neural basis of these crossmodal effects in humans remains unknown. It has generally been assumed that they affect only multimodal neural structures (5–7), but recent accounts suggest that back-projections from multimodal areas to unimodal areas may play a role (8–10).

We used event-related functional magnetic resonance imaging (fMRI) (11) to test whether tactile stimuli can spatially influence unimodal visual areas via back projections. On each trial, the participants (12) received visual targets in either the left or right hemifield in a manner that was unpredictable. On a randomly chosen half of the trials, this visual stimulus was coupled with concurrent tactile stimulation to the right hand (i.e., at the same external location as any right visual stimulation) (13). Four event types were or-

ganized in a 2 by 2 factorial design. One factor was the side of visual stimulation (right or left). The second factor was the occurrence of right tactile stimulation (present or absent). Our analysis first established the effect of lateralized visual stimulation on contralateral occipital areas. We then tested whether responses within these areas were modulated by the presence of tactile stimulation (14).

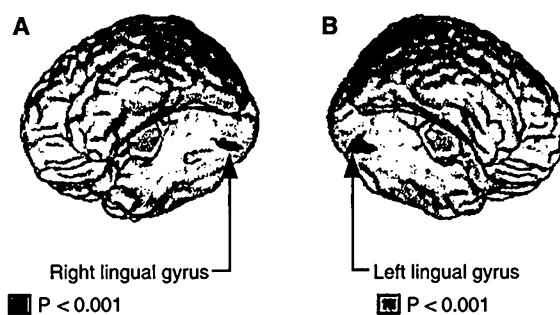
Figure 1 shows activations due to the side of the peripheral visual stimulation. As expected, activations were found in contralateral occipital areas. The main effect of left hemifield visual stimulation was a cluster of activation in the posterior part of the right lingual gyrus, contralateral to the visual targets. The maximum activation was at  $x, y, z = 30, -84, -14$  (Z score = 4.8;  $P$ -corrected = 0.005). The reverse comparison showed

that stimulation in the right hemifield also activated the posterior part of the lingual gyrus, now in the left hemisphere ( $x, y, z = -24, -74, -10$ ; Z score = 5.1;  $P$ -corrected < 0.001) (15).

These symmetrical activations in the lingual gyri define a brain response that is sensitive to the side of our visual stimulation. We then examined the effect of concurrent right tactile stimulation on these contralateral responses by testing for the interaction between the side of the visual stimulation and the presence of touch. The analysis revealed amplification of visual response to lights on the right side by touch on the same side. The left lingual gyrus showed a significant interaction, with the maximum at  $x, y, z = -18, -82, -6$  (Z score = 3.2,  $P$ -corrected = 0.044) (Fig. 2). Thus, the left lingual gyrus not only responded to right visual stimulation, but did so more strongly with concurrent tactile stimulation on the right (compare red curve with blue curve in left graph of Fig. 2C). Such modulation was not simply due to this brain area responding directly to touch. The crossmodal amplification was spatially specific because bimodal stimulation that was spatially incongruent (i.e., adding right tactile to left visual stimulation) did not cause any signal increase in the same area (see magenta curve in right graph of Fig. 2C).

By contrast, in the right lingual gyrus, responses to left visual stimuli tended to show a reverse pattern of suppression by right touch, though this was not significant. In a follow-up study, tactile stimulation was delivered to the left hand instead. This produced mirror-image results with significant cross-

**Fig. 1.** Effect of side of the visual stimulation. The effect of peripheral visual stimulation was projected on a rendered view of the canonical MNI brain template. The cerebellum was removed and the brain was tilted to allow a direct view of the ventral surface of the occipital lobes. (A) Main effect of left versus right visual stimulation. Comparison of left versus right events (with and without tactile stimulation) revealed activation of the right lingual gyrus, contralateral to the visually stimulated side. The right middle and superior occipital gyri showed a similar trend. (B) Main effect of right versus left visual stimulation. This comparison also revealed activation of the lingual gyrus, now in the left hemisphere, contralateral to the stimulated hemifield. The cluster was symmetrical to the ventral activation observed in the right hemisphere for the opposite comparison. Additionally, significant contralateral responses were observed (15) in the left middle and superior occipital gyri (not visible in this projection).



<sup>1</sup>Institute of Cognitive Neuroscience, University College London, UK. <sup>2</sup>Wellcome Department of Cognitive Neurology, Institute of Neurology, London, UK.

\*To whom correspondence should be addressed. E-mail: e.macaluso@fil.ion.ucl.ac.uk